Phase Transformations in Ti-6Al-4V–*x*H Alloys

J.I. QAZI, O.N. SENKOV, J. RAHIM, A. GENC, and F.H. (SAM) FROES

Microstructures, phases, and phase transformations in Ti-6Al-4V alloy specimens containing 0, 10, 20, and 30 at. pct hydrogen were investigated using optical microscopy (OM), transmission electron microscopy (TEM), X-ray diffraction (XRD), and microhardness testing. Alloying with hydrogen was achieved by holding the specimens in a pure hydrogen atmosphere of different pressures at 780 °C for 24 hours. The phases present in the temperature range of 20 °C to 1000 °C were determined by microstructural characterization of the specimens quenched from different temperatures. Increasing the hydrogen addition from 0 to 30 at. pct lowered the beta-transus temperature of the alloy from 1005 °C to 815 °C, significantly slowed down the kinetics of the beta-to-alpha transformation, and led to formation of an orthorhombic martensite instead of the hexagonal martensite found in quenched specimens containing 0 pct H. A hydride phase was detected in specimens containing 20 and 30 at. pct hydrogen. The time-temperature-transformation (TTT) diagrams for beta-phase decomposition were determined at different hydrogen concentrations. The nose temperature for the beginning of the transformation decreased from 725 °C to 580 °C, and the nose time increased from 12 seconds to 42 minutes when the hydrogen concentration was increased from 0 to 30 at. pct.

I. INTRODUCTION

TITANIUM and conventional titanium alloys have a high affinity for hydrogen and are capable of absorbing up to 60 at. pct hydrogen at 600 °C, and even higher contents can be alloyed with titanium at lower temperatures.[1] The fact that hydrogen can be added by exposing the titanium samples to a hydrogen environment at elevated temperatures and can then be easily removed by a simple vacuum annealing makes it a unique temporary alloying element.[1–12] Hydrogen as an alloying element changes the phase compositions and kinetics of the phase transformations in titanium alloys, allowing novel thermal and thermomechanical treatments. As a result, novel microstructures and enhanced mechanical properties can be obtained after the thermohydrogen processing (THP).[1–12] At sufficiently high hydrogen concentrations, room-temperature embrittlement provides an economic method for the production of titanium powder (the hydride-dehydride (HDH) process), with the hydrogen then removed by a simple vacuum anneal. Temporary alloying of hydrogen with Ti-6Al-4V, the most popular $\alpha + \beta$ alloy accounting for more than half of all titanium sales, has been of interest in a number of investigations,[10–18] because improved workability and refined microstructures can be achieved, which are not possible otherwise.[1,10–12,19,20]

An improvement in superplastic forming of Ti-6Al-4V has been achieved by temporary alloying with hydrogen.[13,17,21] A reduction of 30 pct in flow stress or a lowering of the forging temperature by 80 °C using 13 to 16 at. pct hydrogen has been reported by Kerr *et al.*[10] Zwicker *et al.* have also reported an improvement in the forgeability of titanium alloys when temporarily alloyed with hydrogen.[22] Ultrafine equiaxed grains can also be produced in Ti-6Al-4V by temporary alloying with hydrogen, leading to an improvement in mechanical properties.[11,15] Although the benefits of temporary alloying of Ti-6Al-4V with hydrogen are numerous, the phase transformations in the system have not been studied extensively. Ti-6Al-4V–hydrogen phase diagrams have been suggested by Kerr *et al.*[10] and Ilyn *et al.*[12] (Figure 1), which are essentially different. Based on their optical microscopy (OM) and X-ray diffraction (XRD) analyses, Kerr *et al.*[10] have proposed a hydride-phase formation by a eutectoid transformation of the beta phase near 800 °C (Figure 1(a)), which is a considerable departure from the pure titanium-hydrogen system, in which the eutectoid transformation occurs 500 °C lower, at 300 °C.[23] On the other hand, Ilyn *et al.*[12] have suggested a phase diagram with a hydride phase present only below 300 °C and a wide $\alpha + \beta$–phase range present above 300 °C (Figure 1(b)). It is clear that detailed additional study is required to determine the correct equilibrium-phase diagram.

In order to fully define the effect of heat treatment on the hydrogenated alloy, nonequilibrium time-temperature-transformation (TTT) diagrams are required at different hydrogen concentrations. However, only one TTT diagram for the beta-phase decomposition (β-TTT diagram) is available: that for the alloy with 40 at. pct hydrogen.[10] However, the authors themselves[10] have questioned the validity of the results. The present work was aimed at obtaining a detailed understanding of the effect of hydrogen as an alloying element on equilibrium and nonequilibrium phase transformations and microstructural evolution in cast Ti-6Al-4V. The Ti-6Al-4V–hydrogen phase diagram was determined using the OM, transmission electron microscopy (TEM), and XRD techniques and was compared with the previously suggested diagrams. The nonequilibrium β-TTT diagrams were also determined for the alloys with 10, 20, and 30 at. pct H.

J.I. QAZI, Postdoctoral Candidate, and J. RAHIM, Master's Student, Department of Materials Science and Engineering, and F.H. (SAM) FROES, Director, Institute for Materials and Advanced Processes, and Chair, Department of Materials, Metallurgical, Mining and Geological Engineering, are with the University of Idaho, Moscow, ID 83844-3026. O.N. SENKOV, Senior Scientist, is with UES, Inc., Dayton, OH 45432-1894. A. GENC, Postdoctoral Student, is with the Metallurgical Engineering Department, Istanbul Technical University, 80626 Maslak-Istanbul, Turkey.

Manuscript submitted October 27, 2000.

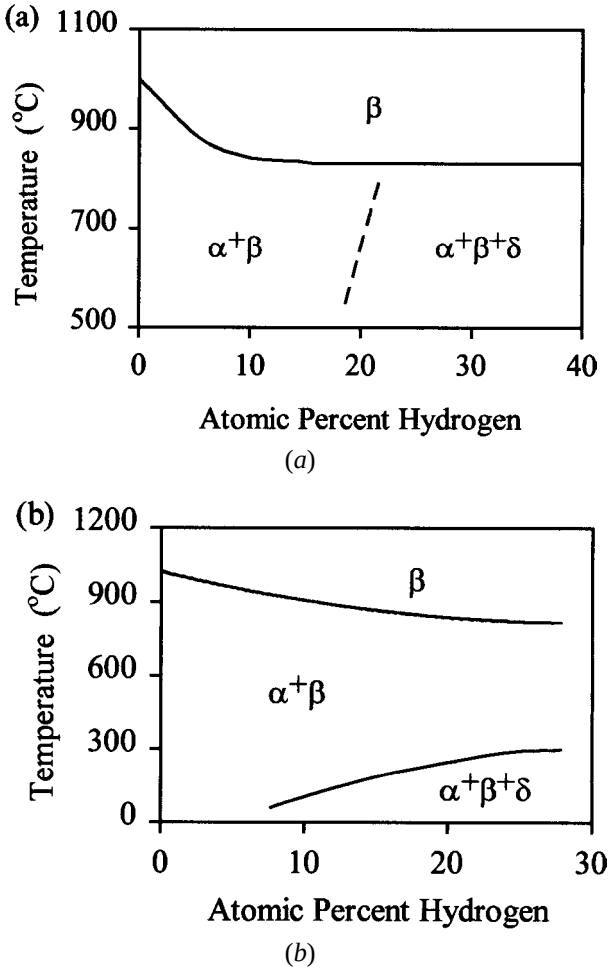

Fig. 1—Phase boundaries in Ti-6Al-4V–hydrogen system according to (*a*) Kerr *et al.*[10] and (*b*) Ilyin *et al.*[12]

Table I. Chemical Composition of the Ti-6Al-4V Plate

Element	Al	V	O	N	H	Ti
Wt pct	6.05	4.06	0.17	0.025	0.0045	balance

II. EXPERIMENTAL

A cast and hot isostatically pressed (at 890 °C) 8-mm-thick Ti-6Al-4V alloy plate with the chemical composition shown in Table I was provided by Precision Castparts Corporation (Portland, OR). Specimen bars of 8 mm in width and 70 to 75 mm in length were hydrogenated by holding at 780 °C in a pure hydrogen atmosphere for 24 hours, following a procedure described elsewhere.[24] A powdered high-purity titanium hydride was used as a source of pure hydrogen for this purpose. Specimens to be hydrogenated were placed in a container made of a 0.2-mm-thick titanium sheet. The container was then placed inside a stainless steel chamber under a vacuum of 40 mtorr before hydrogenation to reduce the impurities from the atmosphere. The stainless steel chamber was then placed in a preheated Hevi Duty Electric Co. furnace, model M-3024, at 780 °C. To vary the hydrogen content, different amounts of titanium hydride were decomposed. After hydrogenation, the specimens were cooled to room temperature by removing the closed stainless steel chamber from the furnace. The hydrogen levels of 10, 20, and 30 at. pct produced in this way were determined by weighing the specimens before and after hydrogenation to the nearest 0.01 mg[10–12,24] and were reconfirmed by weighing samples before and after dehydrogenation, which was performed in a vacuum at 750 °C for 4 hours. The weight gain as a result of hydrogenation was the same as the weight loss after dehydrogenation, indicating that only hydrogen was picked up and removed, and no significant amount of oxygen and/or nitrogen pickup occurred.

The β-transus temperature was determined metallographically by holding specimens at different temperatures for 1 hour in air using a Lindberg tube furnace followed by water quenching. The oxide layer which formed on the surface of the samples retained the hydrogen inside the samples during heating up to 940 °C, in agreement with References 10 and 24. Microstructural examination was carried out using an Olympus PMG 3 optical microscope (Leco Corporation, Warrendale, PA). The samples for OM were mechanically polished and etched in a solution consisting of 5 mL hydrogen peroxide, 2 mL hydrofluoric acid (50 pct), and 100 mL distilled water. Phase analysis was performed using TEM (JEOL*-JEM 2010) and XRD (Siemens 5000) techniques.

*JEOL is a trademark of Japan Electron Optics Ltd., Tokyo.

The 3-mm-diameter thin foils for TEM were electropolished using a twin-jet electropolisher at 50 V in a solution bath consisting of 300 mL methanol, 175 mL 2-butanol, and 30 mL perchloric acid (70 pct), as recommended by Blackburn and Williams.[25] Hydrogen evolution in the thin foils during electropolishing was avoided by keeping the temperature of the electrolytic bath between −50 °C and −60 °C.[26]

To determine the kinetics of the beta-phase decomposition at different temperatures (β-TTT diagrams) for each hydrogen concentration, specimens were heated above the β-transus temperature for 1 hour, placed in a furnace at lower temperatures for varying times, and then water quenched. The volume fractions of the $\alpha + \delta$ phases were determined after different annealing temperatures and times using OM, and the time for the transformation start was identified at each temperature as the time corresponding to 5 vol pct transformation. The microhardness of specimens was measured by applying a load of 500 g for 20 seconds using a LECO* M400G Vickers hardness unit.

*LECO is a trademark of the LECO Corporation, St. Joseph, MI.

III. RESULTS

A. *Microstructure after Hydrogenation*

The cast and hot-isostatic pressed (HIP'd) Ti-6Al-4V plate had a coarse alpha-beta lamellar structure, with an average prior-beta grain size of 0.97 mm and an average interlamellar α spacing of 5 μm (Figure 2(a)). After hydrogenation, the prior-beta grain size remained unchanged; however, an addition of 10 at. pct H led to the formation of a martensitic structure (both hexagonal α' and orthorhombic α'', as identified by TEM; details provided subsequently), shown in Figure 2(b), and a considerable decrease in the lamellar spacing to less than 1 μm, in this case, of α, α', and α'' laths. The martensitic structure can be identified in Figure 2(b) as smooth (etch-resistant) regions between the alpha lamellae.

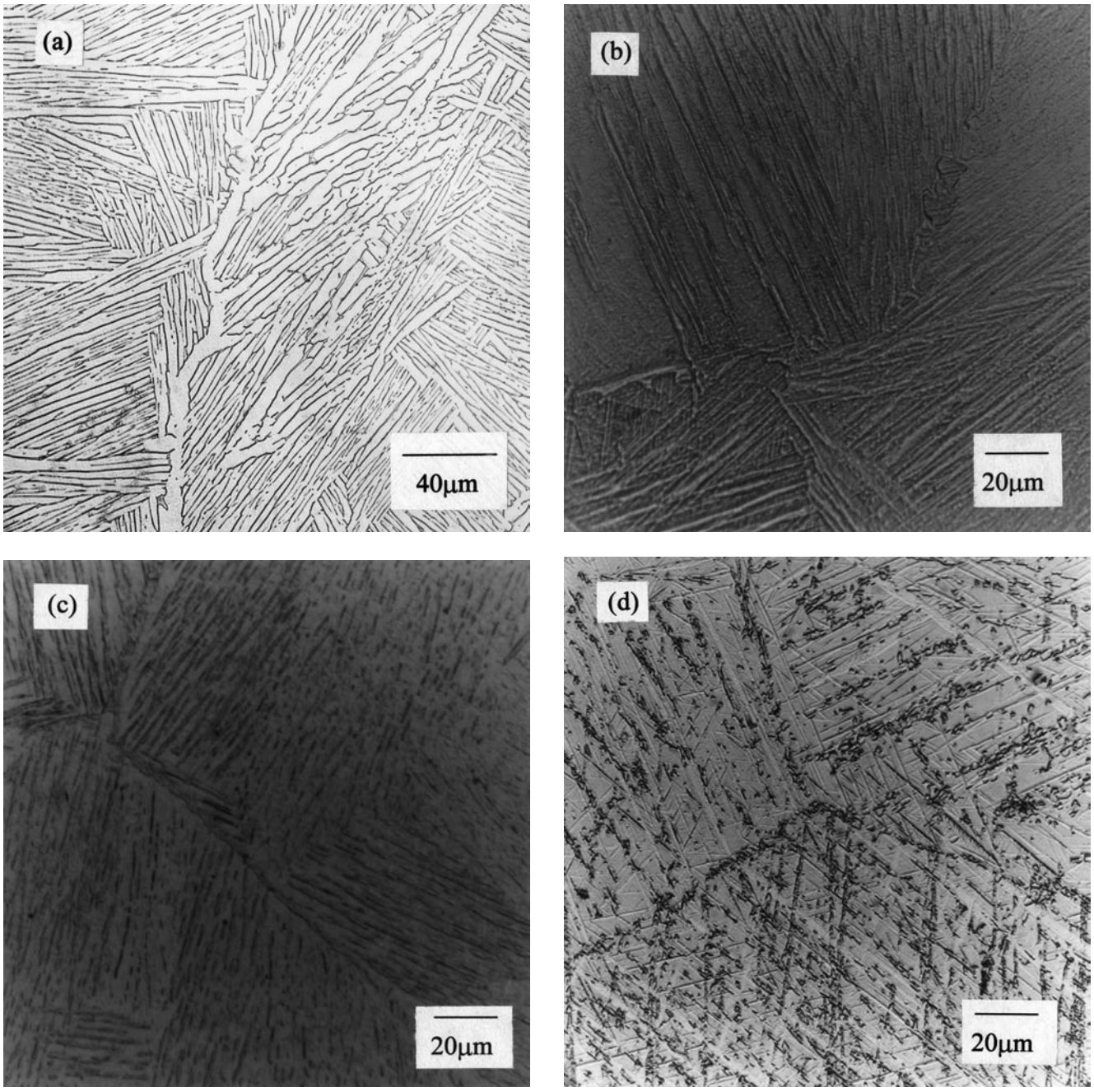

Fig. 2—Microstructure of the Ti-6Al-4V alloy in (*a*) as-cast and HIP'd condition and (*b*) through (*d*) after hydrogenation to (b) 10 at pct H, (*c*) 20 at. pct H, and (*d*) 30 at. pct H at 780 °C for 24 h followed by air cooling.

The volume fraction of the martensite increased from 30 to 80 vol pct, and transformation of the alpha lamellae into chains of fine equiaxed particles occurred when the hydrogen concentration increased from 10 to 30 pct (Figures 2(c) and (d)). The XRD analysis indicated that the nonhydrogenated specimens contained primarily alpha phase and less than 7 pct of beta phase (Figure 3(a)). After hydrogenation, additional peaks from the orthorhombic α'' martensite were detected and the peaks from the hexagonal α phase became wider (Figures 3(b) through (d)). The peak widening was evidently caused by the presence of the hexagonal α' martensite, with lattice parameters that differed only slightly from the lattice parameters of the α phase due to the composition variations in these phases.[27] The XRD results were supported by the TEM analysis, which showed alpha lamellae with a low dislocation density ($\sim 10^8$ cm^{-2}) and thin beta laths between the alpha lamellae in the as-cast and hipped alloy (Figure 4). Additionally, a fine martensitic structure was detected in the hydrogenated specimens (Figure 5). The α' martensite laths were distinguished from the original α lamellae by a high dislocation density and a higher concentration of vanadium, while the α'' martensite laths were distinguished by the presence of fine twins inside them and the orthorhombic lattice structure.[28] Figure 5(a) is a bright-field (BF) image of α' and α'' laths in the specimen containing 10 at. pct hydrogen, Figure 5(b) is the corresponding selected-area diffraction pattern (SADP) with zone axes of $[\bar{1}2\bar{1}3]_{\alpha'}$ and $[\bar{1}\bar{1}2]_{\alpha''}$, and Figure 5(c) is the indexed SADP

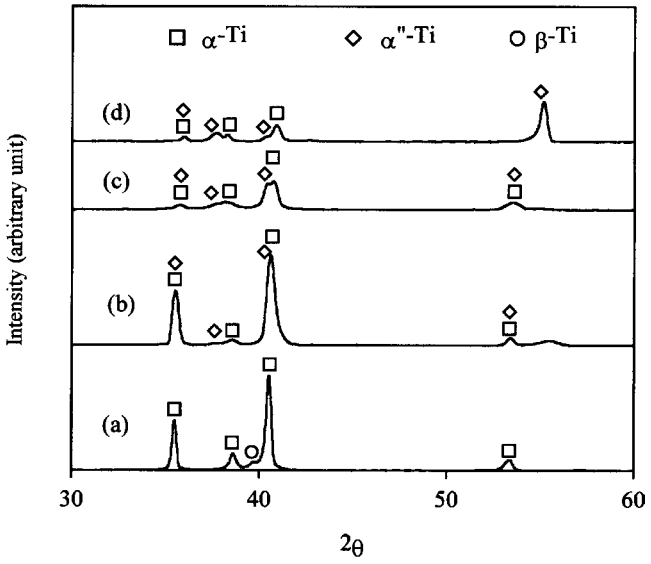

Fig. 3—X-ray diffraction patterns of the Ti-6Al-4V alloy in (*a*) as-cast and HIP'd condition and (*b*) through (*d*) after hydrogenation to (*b*) 10 at. pct H, (c) 20 at. pct H, and (d) 30 at. pct H at 780 °C for 24 h followed by air cooling.

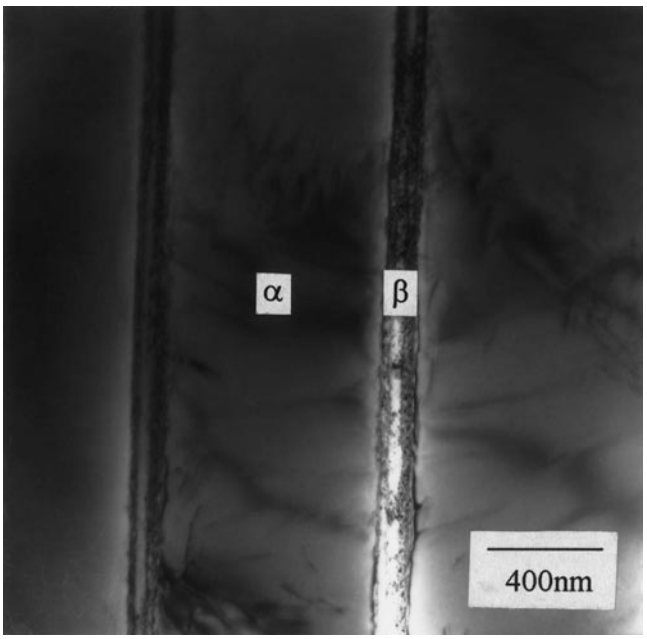

Fig. 4—TEM photomicrograph of alpha lamellae and thin beta laths in the cast and HIP'd Ti-6Al-4V alloy.

in Figure 5(b), which reveals the orientation relationship of the adjacent martensite laths to be $(1\bar{1}01)_{\alpha'} \parallel (021)_{\alpha''}$. No hydride phase was detected in specimens containing 10 at. pct hydrogen; however, the TEM analysis does reveal the presence of the fcc-δ titanium hydride phase in the specimens containing the higher hydrogen concentrations of 20 or 30 at. pct. Figure 6(a) is a TEM BF image of the δ-hydride twins and α' laths in a specimen containing 20 at. pct H; Figure 6(b) is the corresponding SADP, which shows the diffraction zones of $[\bar{1}2\bar{1}3]_{\alpha'}$, $[011]_{\delta}$, and $[0\bar{1}\bar{1}]_{\delta}$; and Figure 6(c) is the indexed SADP in Figure 6(b), which reveals the orientation relationship of adjacent twinned regions to be

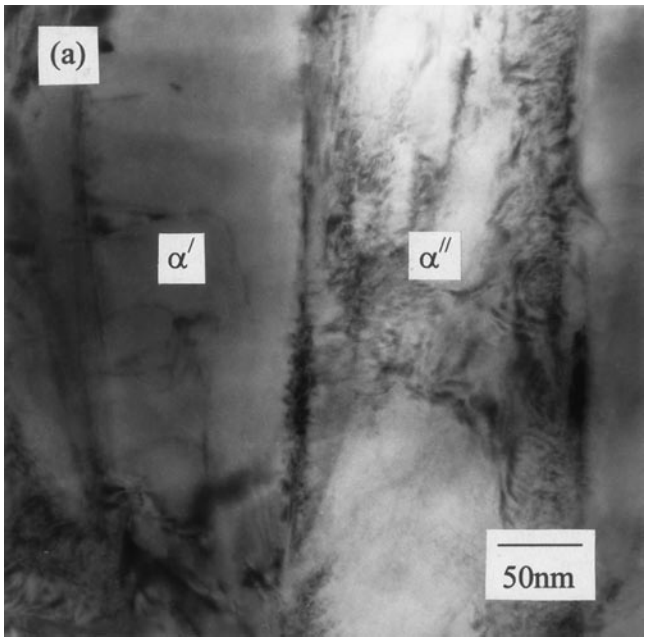

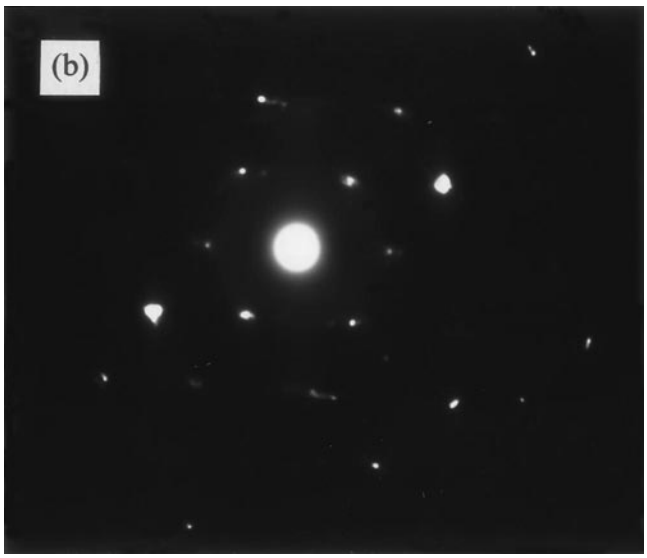

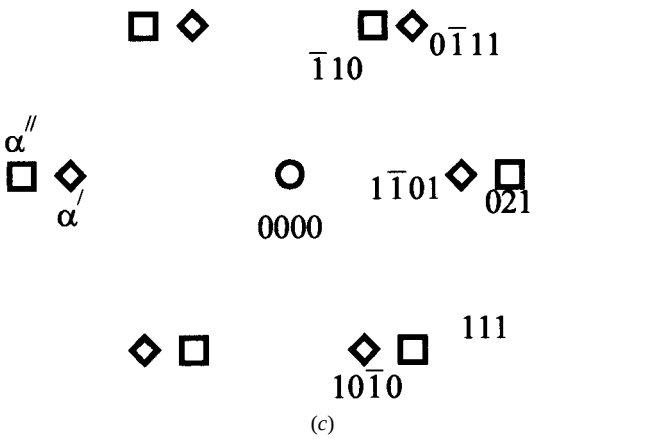

(*c*)

Fig. 5—(*a*) BF image showing α' and α'' martensite laths, (*b*) corresponding SADP, and (*c*) indexed SADP shown in (b). Zone axes are $[\bar{1}2\bar{1}3]_{\alpha'}$ and $[\bar{1}\bar{1}2]_{\alpha''}$ and $(1\bar{1}01)_{\alpha'} \parallel (021)_{\alpha''}$. The Ti-6Al-4V alloy with 10 at. pct H.

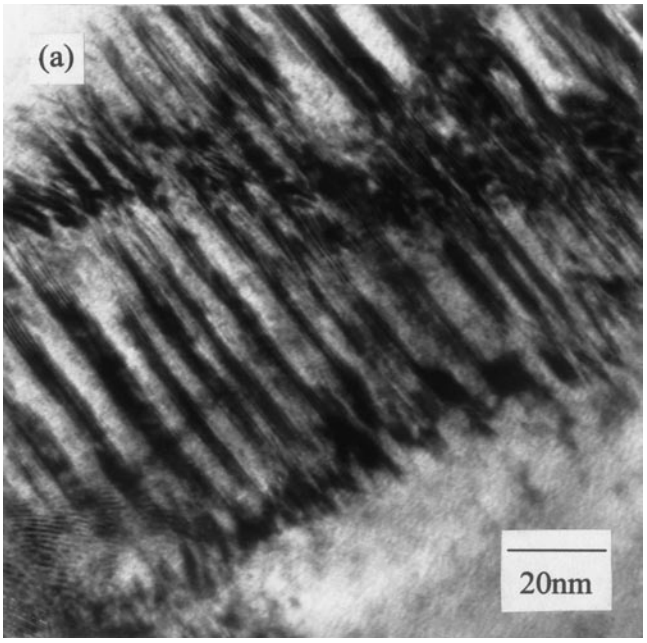

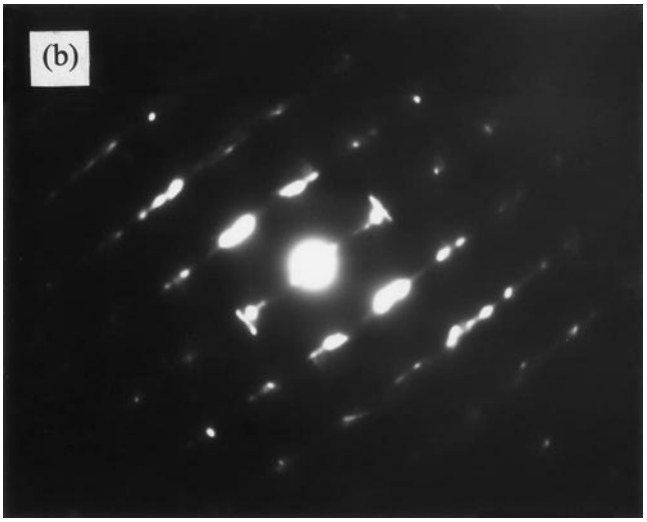

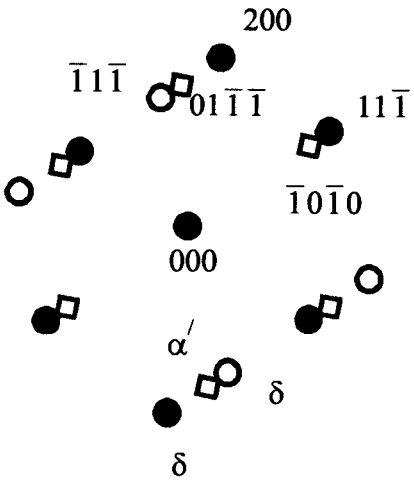

(*c*)

Fig. 6—(*a*) BF showing α' martensite and δ hydride laths, (*b*) corresponding SADP, and (*c*) indexed SADP shown in (b). Zone axes are $[1\bar{2}\bar{1}3]_{\alpha'}$, $[011]_{\delta}$, $[0\bar{1}\bar{1}]_{\delta}$. The Ti-6Al-4V alloy with 20 at. pct H.

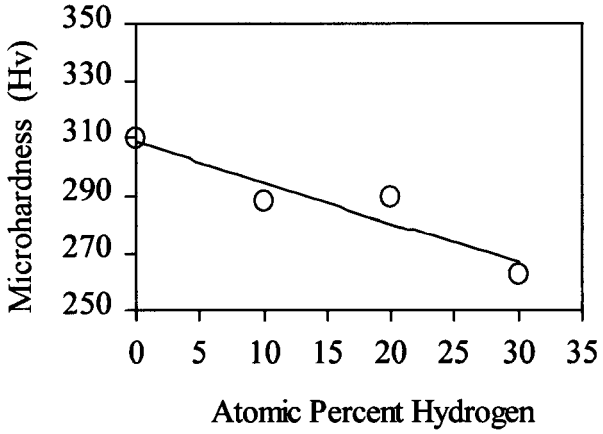

Fig. 7—Microhardness of Ti-6Al-4V hydrogenated specimens as a function of the hydrogen concentration.

$[011](11\bar{1})_{\delta M} \parallel [0\bar{1}\bar{1}](11\bar{1})_{\delta T}$ and of α' and δ laths to be $[10\bar{1}0](0001)_{\alpha'} \parallel [11\bar{1}](1\bar{1}0)_{\delta}$. The microhardness of the hydrogenated specimens decreased slightly with an increase in the hydrogen concentration (Figure 7), resulting from an increased amount of the soft orthorhombic α'' martensite.[27]

B. *Effect of Hydrogen on Beta-Transus Temperature*

The effect of annealing temperature on the microstructure of specimens containing 30 at. pct H is illustrated in Figure 8. After heating at 750 °C and 800 °C for 1 hour and water quenching, primary alpha particles and a martensite phase were detected, with the volume fraction of the alpha particles decreasing with a temperature increase (Figures 8(a) and 8(b)), indicating that both the samples were annealed below the beta-transus temperature. However, after annealing at 830 °C or 850 °C and water quenching (Figures 8(c) and (d)), only martensite phase was detected, indicating that the annealing was conducted in the beta-phase range, *i.e.*, above the beta-transus temperature. Using this approach, the beta-transus temperature was determined for specimens with different hydrogen concentrations, and the results are shown in Figure 9. A decrease in the beta-transus temperature from 1005 °C to 815 °C occurred with an increase in the hydrogen concentration from 0 to 30 at. pct.

The TEM analysis allowed additional features of the annealed specimens to be identified. Figure 10 is a TEM photomicrograph of a specimen with 10 at. pct H after annealing at 900 °C (above the beta transus) and water quenching. Only α'' martensite laths, and no hydride phase, were detected at this hydrogen content. The hydride phase, in addition to the martensite phase, was detected in specimens with 20 and 30 at. pct H quenched from 850 °C (Figure 11), although the hydride phase was not observed in the 20 at. pct H specimens annealed at 900 °C; both 850 °C and 900 °C are above the beta transus for these hydrogen contents. This indicates that an additional phase field, β(H) + δ, is present above the beta transus at hydrogen concentrations of 20 to 30 at. pct, as shown in Figure 9 by a dashed line.

C. *Kinetics of the Beta-Phase Decomposition (Beta-TTT Diagrams)*

The kinetics of the beta-phase decomposition were determined for specimens with 10, 20, and 30 at. pct H. For this,

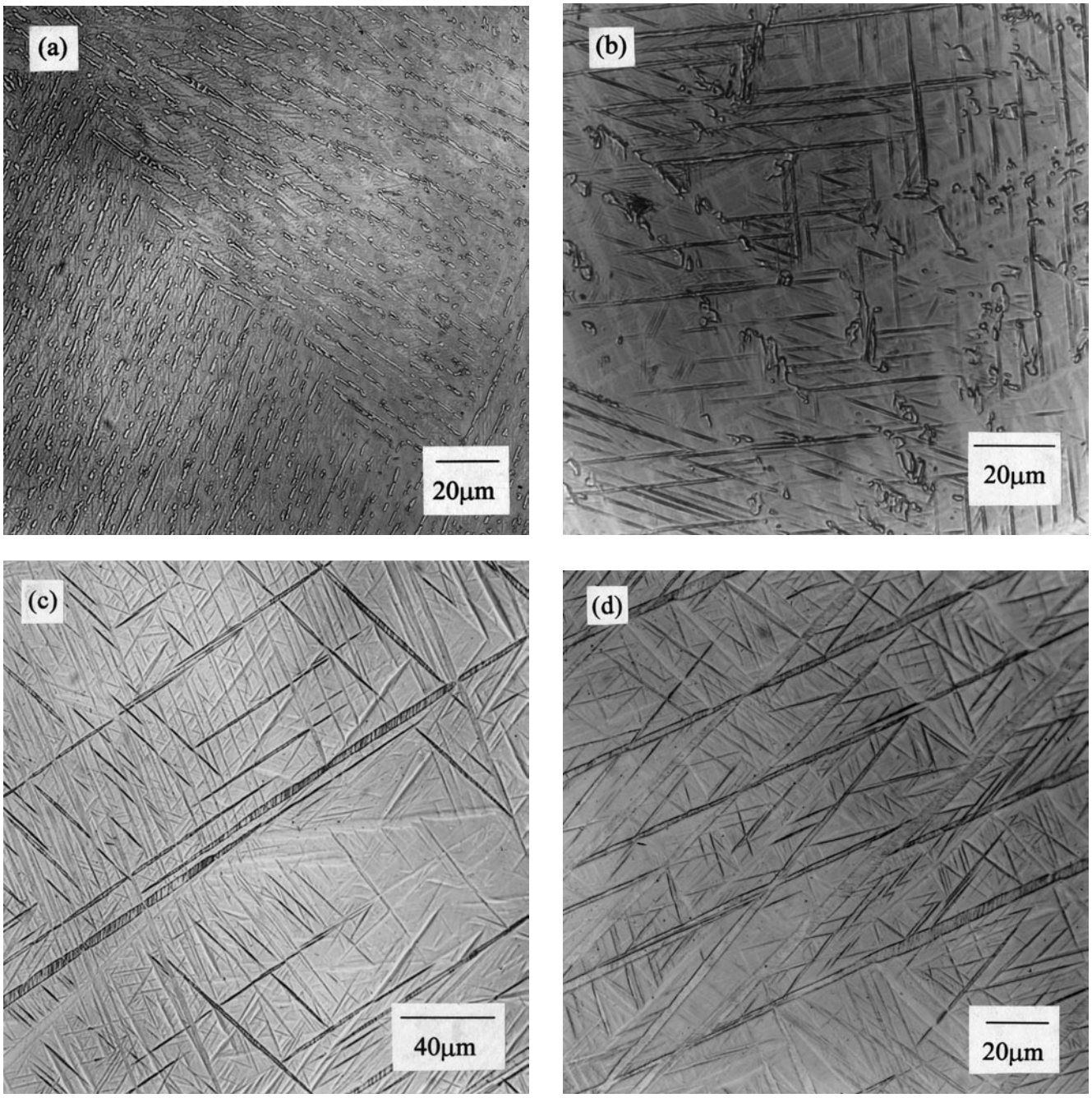

Fig. 8—OM photomicrographs of Ti-6Al-4V alloy specimens containing 30 at. pct H after heating at (*a*) 750 °C, (*b*) 800 °C, (*c*) 830 °C, and (*d*) 850 °C for 1 h and water quenching.

the specimens were annealed for 1 hour above the beta transus, at 890 °C, 855 °C, and 850 °C, respectively, placed in a furnace at different lower temperatures for varying times, then water quenched, and the microstructure was examined using OM and TEM. Figure 12 shows the effect of holding time on the decomposition of the beta phase at 780 °C in specimens with 30 at. pct H. No decomposition of the beta phase occurred after 16 hours of holding, and only martensite needles were seen in the quenched specimen (Figure 12(a)). However, about 12 vol. pct α particles along with the martensite needles were detected after a hold of 64 hours, indicating that the start of the beta-to-alpha transformation at this temperature occurred between 16 and 64 hours (Figure 12(b)). After completion of the transformation of the beta phase in specimens with 20 and 30 at. pct H, TEM analysis indicated that the hydride phase was also present; however, no hydride phase was detected in specimens with 10 at. pct H. The nature of the black spots in the center of the alpha particles (Figure 12(b)) is currently unclear. They may be end-on martensite laths acting as nucleation sites for the alpha phase or titanium hydride precipitates; this will be discussed in detail in a later article.

Figure 13 shows the microhardness of specimens with 30 at. pct H after a β solution treatment at 850 °C for 1 hour followed by annealing at 500 °C or 680 °C and water quenching. A very small change in the microhardness was detected

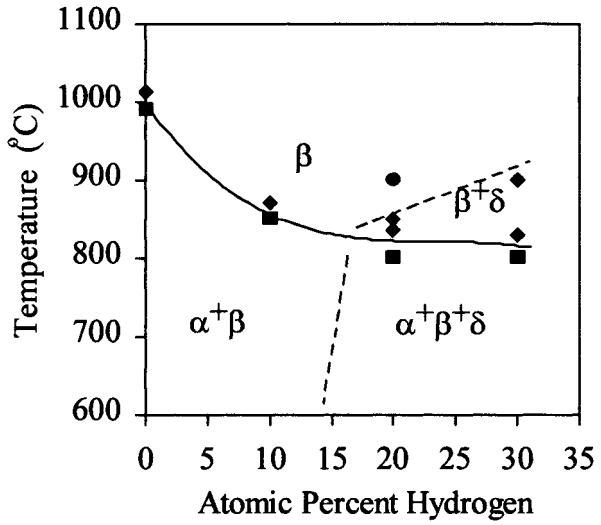

Fig. 9—Phase boundaries in the Ti-6Al-4V–hydrogen system defined in the present work.

at annealing times where no decomposition of the beta phase occurred. Once the beta-phase decomposition started, the microhardness increased rapidly, reaching a maximum and then decreasing for longer annealing times. The increase in the microhardness was evidently due to the decomposition of the beta phase into hcp α phase during annealing; the latter is harder than the orthorhombic α'' martensite formed from the beta phase during quenching. The maximum hardness reached at a given annealing temperature has been attributed to the completion of the beta-to-alpha transformation.[29] The same approach has been used to determine the completion of the transformation for the samples annealed at different temperatures with different hydrogen concentrations.

The TTT diagrams for specimens containing 10, 20, and 30 at. pct H are shown in Figure 14. The curves for the beginning of the transformation correspond to a 5 vol pct transformation, and the curves for completion of the transformation correspond to the peak-microhardness annealing time. It can be seen that an increase in the hydrogen concentration decreased the transformation starting nose temperature and increased the transformation starting nose time. Figure 15 illustrates the nose temperature and time as a function of hydrogen concentration. The nose temperature decreases linearly with increasing hydrogen content, according to the following relation (with a regression coefficient of $R^2 = 0.99$):

$$T_N = 731 - 5.0C_H \quad [1]$$

where T_N is the nose temperature in degrees Celsius, and C_H is the hydrogen concentration in atomic percent.

The nose-time increase with an increase in the hydrogen content can be described by a quadratic relation:

$$t_N = 2.8C_H^2 \quad [2]$$

where t_N is the nose time in seconds.

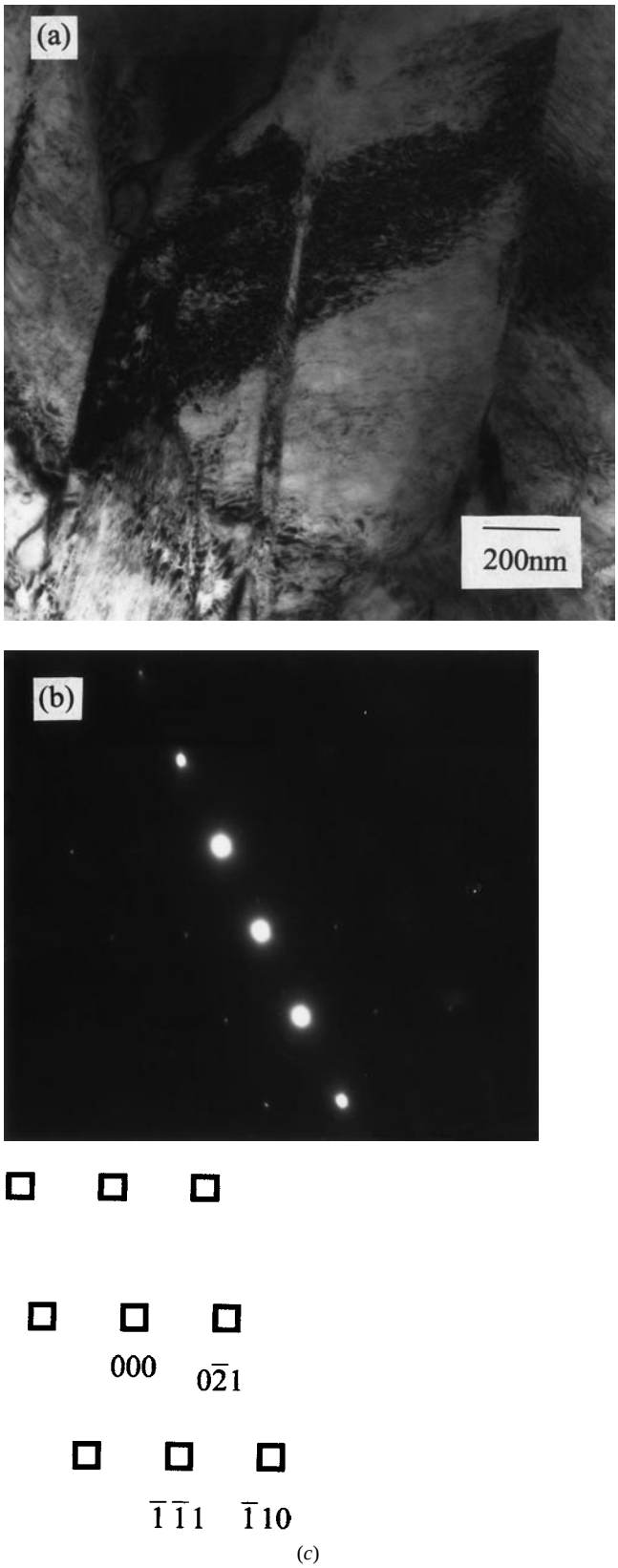

Fig. 10—TEM photomicrograph of a specimen with 10 at. pct H after annealing at 900 °C and water quenching: (*a*) BF, (*b*) SADP with a zone axis of $[112]_{\alpha''}$, and (*c*) indexed SADP shown in (b).

IV. DISCUSSION

A. *Equilibrium Ti-6Al–4V-H Phase Diagram*

On the basis of the microstructural analysis conducted in the present work and results available from the literature, the phase diagram shown in Figure 9 is proposed. In the hydrogen concentration range from 0 to at least 10 at. pct,

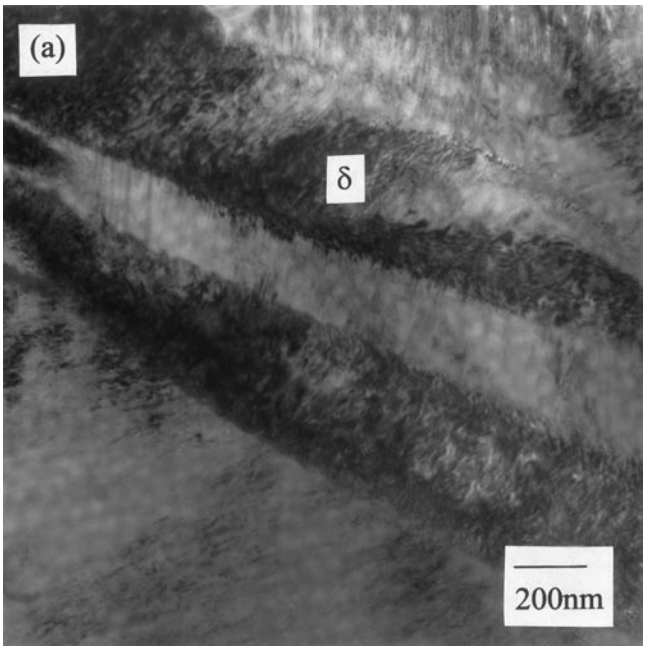

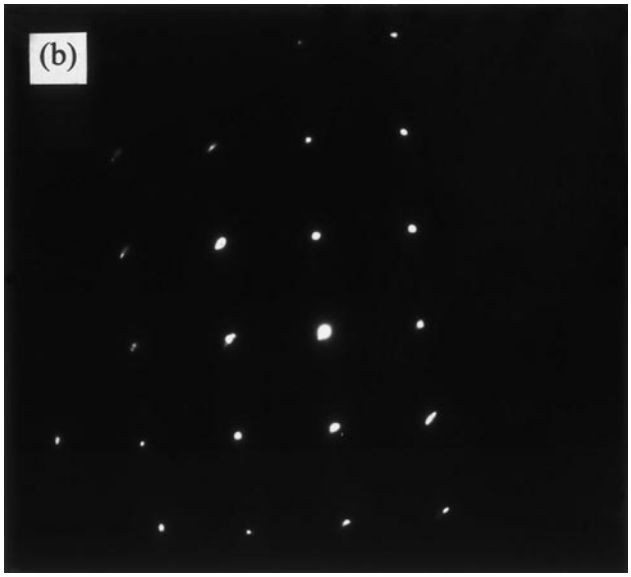

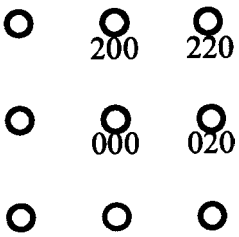

(*c*)

Fig. 11—TEM photomicrograph of a specimen with 20 at. pct H after 1 h annealing at 850 °C and water quenching: (*a*) BF showing titanium hydride laths, (*b*) SADP with a zone axis of $[001]_{\delta}$, and (*c*) indexed SADP shown in (b).

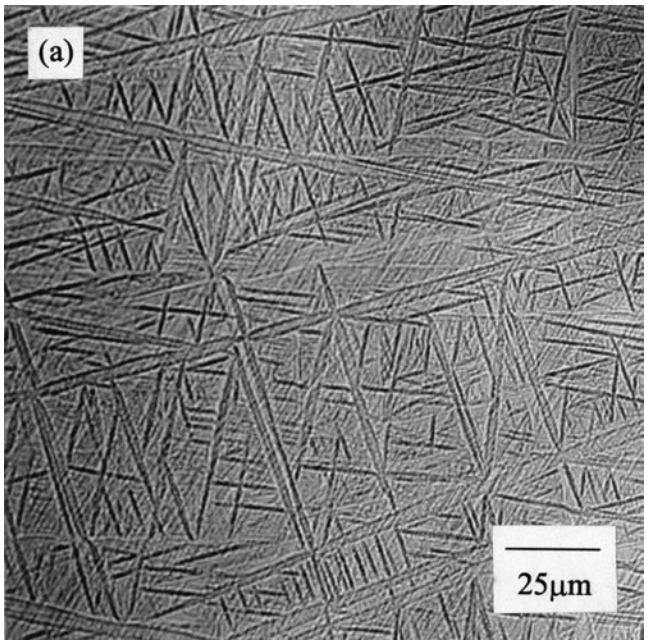

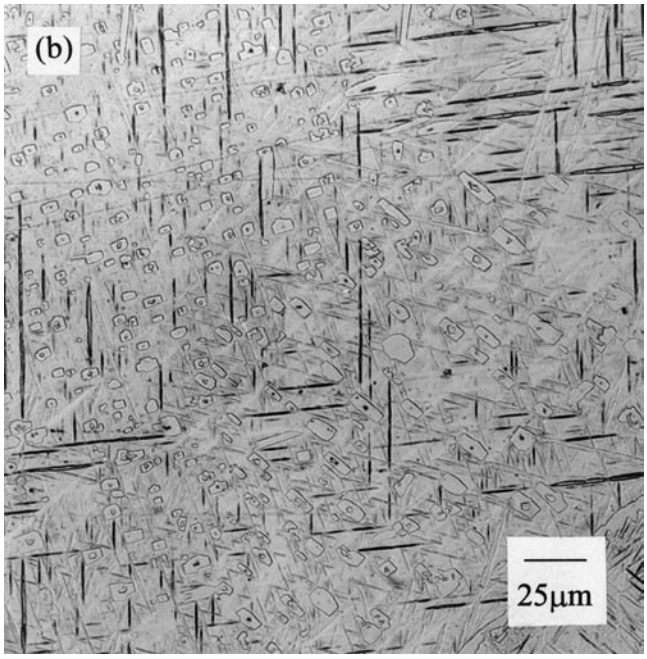

Fig. 12—OM photomicrographs of specimens with 30 at. pct H after annealing at 850 °C for 1 h followed by annealing at 780 °C for (*a*) 16 h and (*b*) 64 h and water quenching, showing 0 and 12 vol. pct transformations, respectively.

no hydride phase is present in the temperature range from 20 °C to 1000 °C, and the hydrogen forms interstitial solid solutions in the alpha and beta phases. The beta-transus temperature decreases rapidly with an increase in the hydrogen concentration, the volume fraction of the beta phase in the alpha + beta–phase range increases, and the hydrogen is concentrated in the beta phase in this concentration range. These findings agree well with the results reported by Kerr *et al.*[10] and Ilyin *et al.*[12] (Figure 1). At higher hydrogen concentrations, the present results do not agree with the diagram suggested by Ilyin *et al.*;[12] however, the results support and expand the diagram suggested by Kerr *et al.*[10] At hydrogen concentrations above ~15 at. pct, a hydride phase is detected and a three-phase range, alpha + beta + hydride, is present below the beta transus, in agreement with Reference 10. An additional two-phase (beta + hydride)

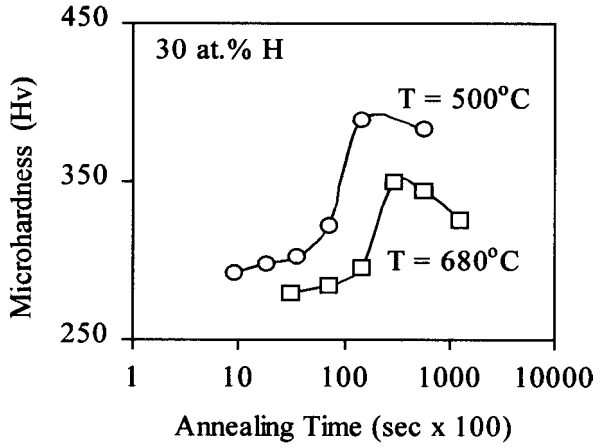

Fig. 13—Dependence of microhardness of specimens with 30 at. pct H on the annealing time at 500 °C and 680 °C. The specimens were beta solution treated at 850 °C for 1 h before annealing and water quenched after annealing.

range is detected above the beta transus in this concentration range in the present work, in contrast to Kerr's work.[10]

B. *Beta-TTT Diagrams and Nonequilibrium Phases*

The results of the present work confirm that hydrogen is an effective beta stabilizer. It decreases the beta-transus temperature[10,12] and also slows the rate of decomposition of the metastable (residual) beta phase during isothermal annealing at temperatures below the beta transus. The addition of each 1 at. pct of hydrogen is found to reduce the nose temperature by about 5 °C and considerably increases the time, in a nonlinear fashion, in accordance with Eq. [2], during which the beta phase remains nontransformed at this temperature (Figure 15). Thus, the nose temperature to begin the transformation decreases from 725 °C[30] to 580 °C, and the nose time increases from 12 seconds[30] to 42 minutes when the hydrogen concentration increases from 0 to 30 at. pct. These results indicate that, with increasing hydrogen contents, lower cooling rates are required to obtain a fully martensite structure and avoid formation of alpha particles; therefore, a more homogeneous structure can be obtained in thicker parts (increased "deep hardenability"). From the beta-TTT diagrams obtained (Figure 14), two critical cooling rates, namely, the minimum cooling rate for formation of 100 pct martensite and the maximum cooling rate below which no martensite is formed, can be estimated from the nose times of the starting and finishing curves of the β-phase decomposition, respectively, assuming that these times are required to pass a 200 °C temperature range. The results are shown in Table II. The estimations show that the minimum cooling rate for the martensite transformation (V_m) is reduced by 20 times with the addition of 10 at. pct H and by 200 times with the addition of 30 at. pct H. Such a large decrease in the critical cooling rate could help to produce a homogeneous microstructure and to avoid warping of quenched structures, which is generally caused by a nonhomogeneous distribution of residual stresses after fast quenching.[27] Table II also shows that the maximum cooling rate (V_d) below which no martensite is formed also decreases with the hydrogen addition, however, not as rapidly as V_m.

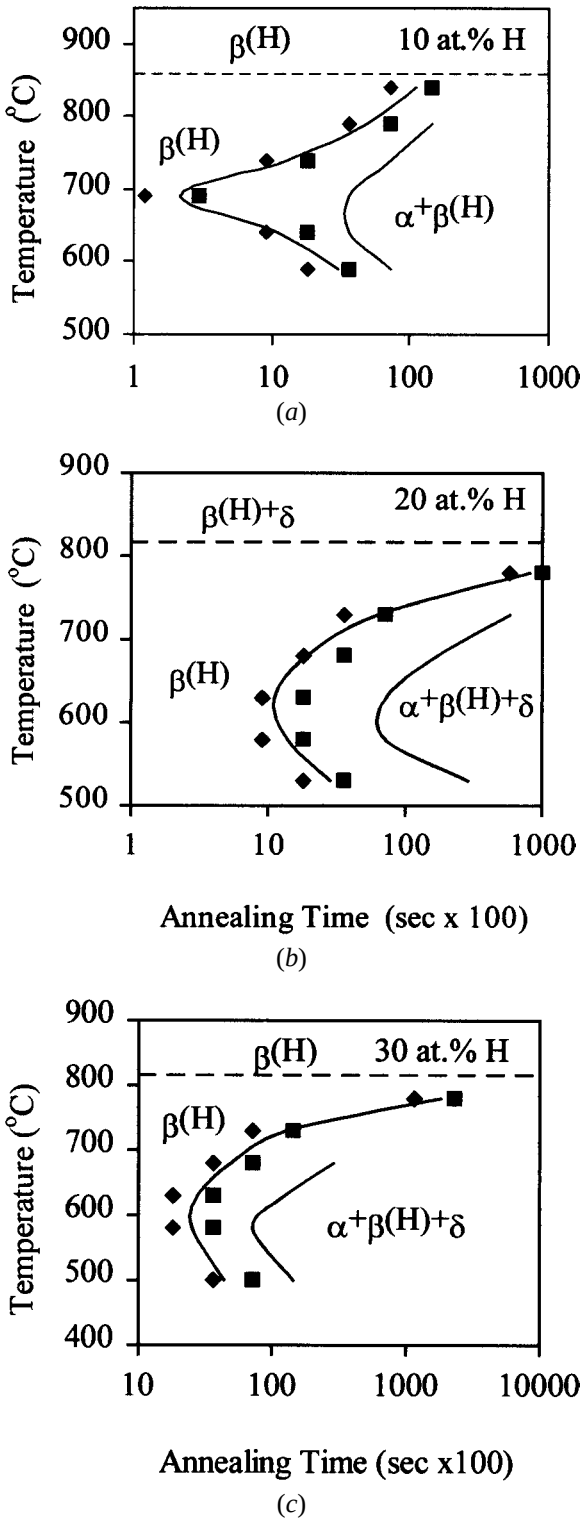

Fig. 14—TTT diagrams for beta phase decomposition in Ti-6Al-4V specimens with (*a*) 10 at. pct H, (*b*) 20 at. pct H, and (*c*) 30 at. pct H.

The difference between V_d and V_m decreases when the hydrogen concentration increases. These findings could be useful in the development of heat-treatment schemes during THP to modify the microstructure and mechanical properties of the alloy.[1,2]

A considerable decrease in the critical cooling rates led to the production of a martensite structure in the hydrogenated

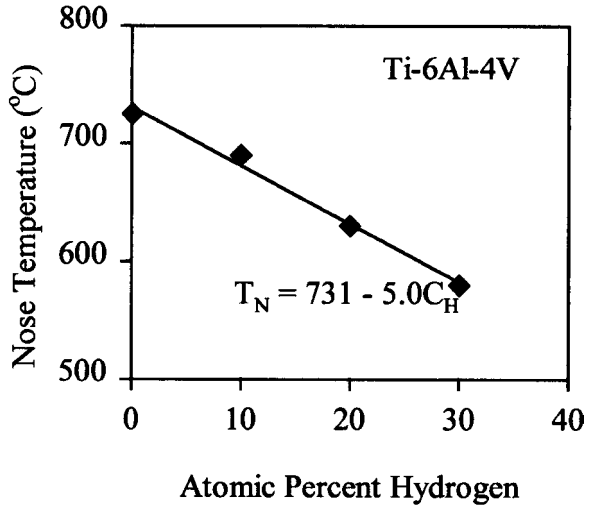

(*a*)

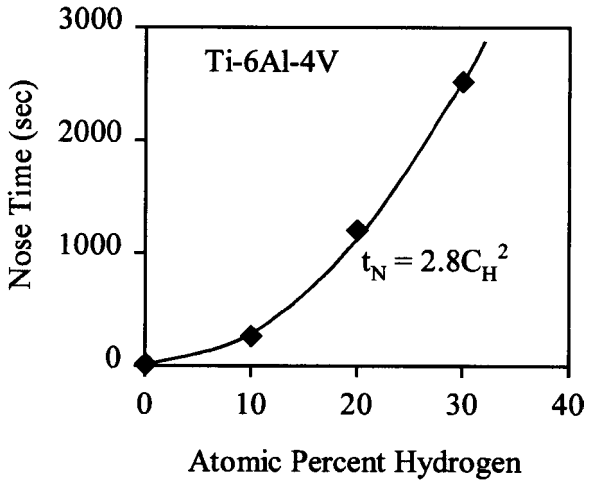

(*b*)

Fig. 15—Dependence of the (*a*) nose temperature and (*b*) nose time for the beginning of the beta phase decomposition on the hydrogen concentration.

Table II. The Minimum Critical Cooling Rate to form 100 Pct Martensite, V_m, and the Maximum Cooling Rate, V_d, below Which No Martensite is Formed in the Ti-6Al-4V Alloy with Different Hydrogen Contents

Hydrogen, At. Pct	0	10	20	30
V_m (°C/min)	1000[27]	50	10	5.0
V_d (°C/min)	30[27]	4	1.5	1.0

specimens after cooling in air or even in a furnace (Figure 2); however, a softer orthorhombic α'' martensite formed instead of the hexagonal α'. This explains the microhardness decrease with an increase in the hydrogen concentration (Figure 7), because the volume fraction of α'' also increases (Figure 3). Formation of the orthorhombic martensite is typical of the $\alpha + \beta$ titanium alloys containing a large amount of beta-stabilizing alloying elements.[27] Therefore, it is not surprising to have a similar effect from the addition of hydrogen, which stabilizes the beta phase. Formation of the orthorhombic martensite in hydrogenated titanium alloys has also been reported in other work.[1,10–12]

V. CONCLUSIONS

1. Phase boundaries were determined in the Ti-6Al-4V–Hydrogen system in the temperature range of 20 °C to 1000 °C and hydrogen-concentration range of 0 to 30 at. pct. In these ranges, three stable phases were identified: hcp alpha, bcc beta, and fcc delta (hydride).
   a. The beta-transus temperature decreases with an increase in the hydrogen concentration from 1005 °C at 0 pct H to 815 °C at 30 pct H. The decrease is rapid at concentrations less than 10 pct H and slows down at higher hydrogen concentrations.
   b. A two-phase alpha + beta field is present at hydrogen concentrations of 0 to 10 at. pct below the beta transus.
   c. A three-phase alpha + beta + delta field is present at hydrogen concentrations above 10 at. pct and below the beta transus.
   d. A two-phase beta + delta field is present at hydrogen concentrations of ≥20 at. pct, above the beta transus and below 900 °C.
2. The TTT diagrams for the isothermal beta-phase decomposition were determined for the Ti-6Al-4V alloys containing 10, 20, and 30 at. pct hydrogen. The beta-phase decomposed into alpha, beta, and hydride phases. It was found that the addition of hydrogen stabilized the beta phase, hence, increasing the time required to begin and end the decomposition.
   a. Alloying with hydrogen increases the nose time and decreases the nose temperature of the TTT start curves. The nose time increases from 12 seconds to 42 minutes and the nose temperature decreases from 725 °C to 580 °C when the hydrogen concentration increases from 0 to 30 at. pct.
   b. The minimum cooling rate for the 100 pct martensite transformation decreases from about 1000 °C/min to 5 °C/min, and the maximum cooling rate below which no martensite transformation occurs decreases from about 30 °C/min to 1 °C/min when the hydrogen concentration increases from 0 to 30 at. pct.

ACKNOWLEDGMENTS

This work was supported by the Army Research Office (Dr. W.M. Mullins), Contract No. DAAG55-98-1-0008. The authors also acknowledge Mr. J. Barrett, Precision Castparts Corporation, for supplying the Ti-6Al-4V castings; Mr. C.F. Yolton, Crucible Research Inc., for specimen hydrogenation; Dr. S.N. Patankar, University of Idaho, and Dr. L.M. Ovecoglu, Istanbul Technical University, for technical discussion and two undergraduate students; Messrs. M.C. Marshal and M.S. Schneider for their help in preparing OM samples.

REFERENCES

1. O.N. Senkov and F.H. Froes: *Int. J. Hydrogen Energy*, 1999, vol. 24, pp. 565-76.
2. O.N. Senkov, J.J. Jonas, and F.H. Froes: *JOM*, 1996, vol. 48, No. 7, pp. 42-47.
3. D. Eylon and F.H. Froes: Patent No. 4,482,398, Nov. 1984.
4. D. Eylon, F.H. Froes, and C.F. Yolton: Patent No. 4,820,360, Apr. 1989.
5. D. Eylon, F.H. Froes, and C.F. Yolton: Patent No. 4,872,927, Oct. 1989.
6. L. Levin, R.G. Vogt, D. Eylon, and F.H. Froes: Patent No. 4,612,066, Sept. 1986.
7. R.G. Vogt, D. Eylon, and F.H. Froes: Patent No. 4,680,063, July 1987.

8. L. Levin, R.G. Vogt, D. Eylon, and F.H. Froes: Patent No. 4,655,855, Apr. 1987.
9. R.J. Smickley and L.E. Dardi: Patent No. 4,505,764, Mar. 1985.
10. W.R. Kerr, P.R. Smith, M.E. Rosenblum, F.J. Gurney, Y.R. Mahajan, and L.R. Bidwell: in *Titanium 80: Science & Technology*, H. Kimura and O. Izumi, eds., TMS, Warrendale, PA, 1980, vol. 4, pp. 2477-86.
11. M. Niinomi, B. Gong, T. Kobayashi, Y. Ohyabu, and O. Toriyama: *Metall. Mater. Trans. A*, 1995, vol. 26A, pp. 1141-51.
12. A.A. Ilyn, B.A. Kolachev, and A.M. Mamonov in *Titanium 92: Science & Technology*, F.H. Froes and I. Caplan eds., TMS, Warrendale, PA, pp. 941-47.
13. T.Y. Fang and W.H. Wang: *Mater. Chem. Phys.*, 1998, vol. 56, pp. 35-47.
14. I. Grimberg, L. Levin, O. Botstein, and F.H. Froes: *J. Mater. Res.*, 1991, vol. 6, pp. 2069-76.
15. H. Yoshimura and M. Hayashi: Nippon Steel Technical Report, 1994, vol. 62, pp. 80-84.
16. D. Eliezer, N. Eliaz, O.N. Senkov, and F.H. Froes: *Mater. Sci. Eng.*, 2000, vol. A280, pp. 220-24.
17. B. Gong, Z. Lai, M. Niinomi, and T. Kobayashi: *Acta Metall. Sinica A*, 1993, vol. 6, pp. 121-24.
18. O.N. Senkov and J.J. Jonas: *Metall. Trans. A*, 1996, vol. 27A, pp. 1877-87.
19. F.H. Froes, D. Eylon, and C. Suryanarayana: *JOM*, 1990, vol. 42, pp. 26-29.
20. H. Yoshimura, K. Kimura, M. Hayashi, M. Ishii, T. Hanamura, and J. Takamura: *Mater. Trans. A, JIM*, 1994, vol. 35, pp. 266-72.
21. B. Gong, C.B. Zhang, and Z.H. Lai: *J. Mat. Sci. Lett.*, 1994, vol. 13, pp. 1561-63.
22. U. Zwicker and H.W. Schleicher: Patent No. 2,892,742, June 1959.
23. A. San-Martin and F.D. Manchester: in *Phase Diagrams of Binary Titanium Alloys*, J.L. Murray, ed., ASM INTERNATIONAL, Materials Park, OH, 1987, pp. 123-25.
24. O.N. Senkov and J.J. Jonas: *Metall. Mater. Trans. A*, 1996, vol. 27A, pp. 1869-76.
25. M.J. Blackburn and J.C. Williams: *Trans. AIME*, 1967, vol. 239, p. 287.
26. J.D. Boyd: *Trans ASM*, 1969, vol. 62, pp. 977-988.
27. R. Boyer, G. Welsch, and E.W. Collings: *Materials Properties Handbook: Titanium Alloys*, ASM INTERNATIONAL, Materials Park, OH, 1994, pp. 490-91.
28. I.J. Polmear: *Light Alloys: Metallurgy of the Light Metals*, 3rd ed., John Wiley and Sons, Inc., New York, NY, 1995, p. 274.
29. F.X.G. Mur, D. Rodriguez, and J.A. Planelli: *J. Alloy Compounds*, 1996, vol. 234, pp. 87-89.
30. C.F. Yolton, F.H. Froes, and R.F. Malone: *Metall. Trans. A*, 1979, vol. 10A, pp. 132-34.